# Developing a platform for Fresnel diffractive radiography with 1 µm spatial resolution at the National Ignition Facility

M. O. Schoelmerich, T. Döppner, C. H. Allen, L. Divol, M. Oliver, D. Haden, M. Biener, J. Crippen, J. Delora-Ellefson, B. Ferguson, D. O. Gericke, A. Goldman, A. Haid, C. Heinbockel, D. Kalantar, Z. Karmiol, G. Kemp, J. Kroll, O. L. Landen, N. Masters, Y. Ping, C. Spindloe, W. Theobald, and T. G. White

**Published version information**

**Citation:** MO Schoelmerich et al. Developing a platform for Fresnel diffractive radiography with 1 µm spatial resolution at the National Ignition Facility. Rev Sci Instrum 94, no. 1 (2023): 013104

**DOI:** 10.1063/5.0101890

Review of Scientific Instruments

# Developing a platform for Fresnel diffractive radiography with 1 μm spatial resolution at the National Ignition Facility

Cite as: Rev. Sci. Instrum. **94**, 013104 (2023); https://doi.org/10.1063/5.0101890
Submitted: 03 June 2022 • Accepted: 04 January 2023 • Published Online: 25 January 2023

M. O. Schoelmerich, T. Döppner, C. H. Allen, et al.







AIP Publishing

Review of Scientific Instruments ARTICLE scitation.org/journal/rsi

# Developing a platform for Fresnel diffractive radiography with 1 $\mu$m spatial resolution at the National Ignition Facility

Cite as: Rev. Sci. Instrum. 94, 013104 (2023); doi: 10.1063/5.0101890
Submitted: 3 June 2022 • Accepted: 4 January 2023 •
Published Online: 25 January 2023



M. O. Schoelmerich,[1,a)] T. Döppner,[1] C. H. Allen,[2] L. Divol,[1] M. Oliver,[3] D. Haden,[2] M. Biener,[1] J. Crippen,[4] J. Delora-Ellefson,[1] B. Ferguson,[1] D. O. Gericke,[5] A. Goldman,[2] A. Haid,[4] C. Heinbockel,[1] D. Kalantar,[1] Z. Karmiol,[2] G. Kemp,[1] J. Kroll,[1] O. L. Landen,[1] N. Masters,[1] Y. Ping,[1] C. Spindloe,[3] W. Theobald,[6] and T. G. White[2]

## AFFILIATIONS

[1]Lawrence Livermore National Laboratory, L-493, 7000 East Avenue, Livermore, California 94550, USA
[2]Department of Physics, University of Nevada, Reno, 1664 N Virginia St., Reno, Nevada 89557, USA
[3]Central Laser Facility, STFC Rutherford-Appleton Laboratory, Chilton OX11 0QX, United Kingdom
[4]General Atomics, P.O. Box 85608, San Diego, California 92186-5608, USA
[5]Centre for Fusion, Space and Astrophysics, Department of Physics, University of Warwick, Coventry CV4 7AL, United Kingdom
[6]Laboratory for Laser Energetics, 250 E River Rd., Rochester, New York 14623, USA

**Note:** This paper is part of the Special Topic on Proceedings of the 24th Topical Conference on High-Temperature Plasma Diagnostics.
[a)]**Author to whom correspondence should be addressed:** schoelmerich1@llnl.gov

## ABSTRACT

An x-ray Fresnel diffractive radiography platform was designed for use at the National Ignition Facility. It will enable measurements of micron-scale changes in the density gradients across an interface between isochorically heated warm dense matter materials, the evolution of which is driven primarily through thermal conductivity and mutual diffusion. We use 4.75 keV Ti K-shell x-ray emission to heat a 1000 $\mu$m diameter plastic cylinder, with a central 30 $\mu$m diameter channel filled with liquid $D_2$, up to 8 eV. This leads to a cylindrical implosion of the liquid $D_2$ column, compressing it to ~2.3 g/cm$^3$. After pressure equilibration, the location of the $D_2$/plastic interface remains steady for several nanoseconds, which enables us to track density gradient changes across the material interface with high precision. For radiography, we use Cu He-$\alpha$ x rays at 8.3 keV. Using a slit aperture of only 1 $\mu$m width increases the spatial coherence of the source, giving rise to significant diffraction features in the radiography signal, in addition to the refraction enhancement, which further increases its sensitivity to density scale length changes at the $D_2$/plastic interface.



## I. INTRODUCTION

The warm dense matter (WDM) state is found in several astrophysical environments, such as planetary interiors or white dwarfs,[1,2] and holds relevance in understanding controlled inertial confinement fusion (ICF).[3] The structure and dynamics of these systems crucially depend on transport properties, such as thermal conductivity, viscosity, and diffusion. For example, Rayleigh–Taylor growth rates are dampened by viscosity and mutual diffusivity.[4–6] In ICF, hydrodynamic instability growth leading to the mixing of ablator material into the fuel and hotspot is one of the leading degradation mechanisms of implosion performance.[4,5]

Theoretical descriptions of plasma transport properties typically have their roots either in the plasma or the condensed matter limits; however, these usually break down in the WDM region. Modeling matter in this parameter regime is particularly challenging as one often encounters systems with strong ion–ion correlations

and electrons that exhibit distinct quantum behavior. To date, only a few experiments have attempted to measure transport properties in the WDM regime, with those that have concentrated on either thermal conductivity[7,8] or viscosity.[9] Recently, there have been promising results at the Linac Coherent Light Source (LCLS) in which inelastic x-ray scattering was used to measure the transport properties in WDM. Fitting the ion component of the experimental spectra using hydrodynamic modeling has allowed the properties of the bulk plasma to be extracted. Unfortunately, these measurements remain bandwidth limited.[9–11]

We have developed a Fresnel diffractive radiography (FDR) platform for the National Ignition Facility (NIF)[12] designed to probe WDM with an unprecedented spatial and temporal resolution. Combining this radiography platform with a cylindrical implosion geometry, we can measure the equation-of-state of compressed matter and potentially determine transport properties, such as thermal conductivity and diffusion. Our platform leverages previous work developing 1D refractive enhanced imaging at the Omega, and NIF lasers,[13,14] and adapts the Fresnel diffractive radiography concept recently demonstrated at the Omega Laser Facility.[15,16] In contrast to previous work on NIF, we have reduced the width of the slit aperture, which defines the x-ray source size, from 5 to 1 $\mu$m to enhance the spatial coherence of the source and hence significantly increase diffraction features.

In the proposed experiments, we use Ti K-shell x-ray emission to isochorically heat a 1000 $\mu$m diameter plastic cylinder with a 30 $\mu$m diameter channel at its center filled with cryogenic (~21 K) liquid $D_2$ (Fig. 1). This sets up a temperature differential between the two materials, with the deuterium initially remaining cold. The resulting pressure difference across the interface triggers a cylindrical implosion, compressing the deuterium column by about 10×, where the final deuterium density is larger than the plastic density. The rapid motion of the interface leads to an outgoing shock wave into the plastic and an incoming rarefaction wave, which can be used to determine the equation of state of these materials. Moreover, after an initial equilibration phase, the evolution across the interface is primarily driven by transport properties, such as thermal conductivity or diffusion. Our experimental platform leverages NIF's outstanding capabilities to produce a macroscopic warm dense matter sample that remains in a steady state for several nanoseconds, enabling the direct measurement of transport coefficients at the material interface.

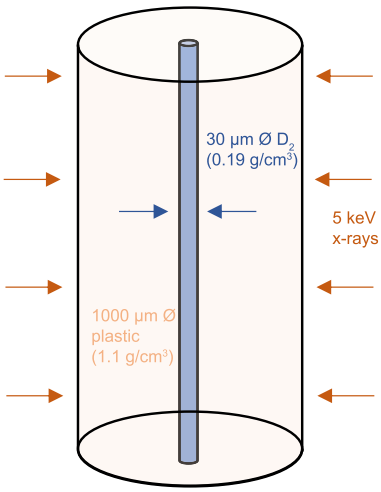


**FIG. 1.** Conceptual design of the physics package. A 30 $\mu$m diameter $D_2$ channel inside a 1000 $\mu$m diameter plastic cylinder is isochorically heated to warm dense matter conditions by ~5 keV x rays, triggering a cylindrical compression of the liquid $D_2$ column to ~10× its original density.

## II. EXPERIMENTAL PLATFORM AT THE NIF

### A. Geometry of the experimental setup

A schematic of the proposed experimental setup at NIF is shown in Fig. 2. The target consists of a 10.8 mm tall, standard Al thermo-mechanical package (TMP) with an inner diameter of about 8 mm, as used in ICF implosions.[12,17] However, instead of containing an Au hohlraum, the TMP holds two 100 $\mu$m thick polyimide containers on each side of the physics package at the center of the target, both encapsulating an annulus of $TiO_2$ foam ($\rho = 12$ mg/cm$^3$). The polyimide containers have an opening (1.5 mm in diameter) along the vertical target axis since the target assembly requires a view along the vertical axis. 176 NIF drive beams (44 quads) pointed through the 4.88 mm laser entrance holes (LEH) of the TMP with a 1 mm diameter focal spot, and a 2 ns square pulse will be used to deliver a total energy of 600 kJ onto the $TiO_2$ foams, subsequently generating around 5 keV Ti K-shell x-ray emission. $TiO_2$ foams

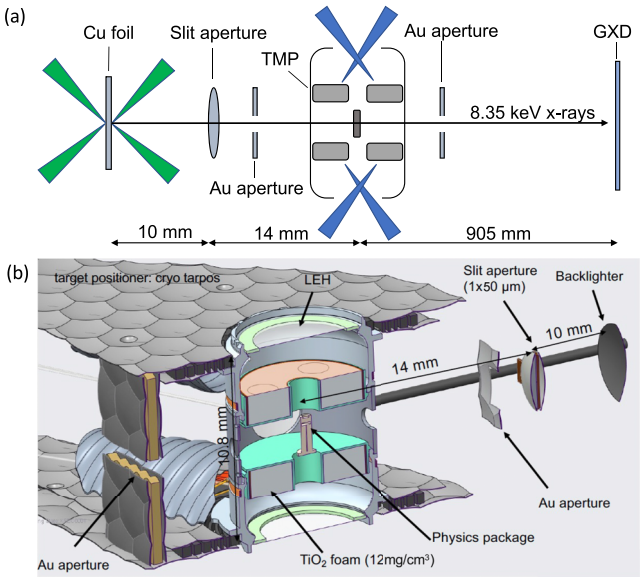


**FIG. 2.** (a) Schematic of the FDR imaging setup. Blue arrows represent drive beams, and green arrows represent backlighter beams. (b) Cut-away of the NIF target: A standard thermo-mechanical package (TMP) holds two $TiO_2$ foam disks on either side of the physics package at the center of the target. A Cu backlighter and a slit aperture are placed next to the TMP with additional Au apertures between the backlighter, target, and diagnostic, which shield against hard x rays from the hohlraum and help collimate the beamprobe x rays.

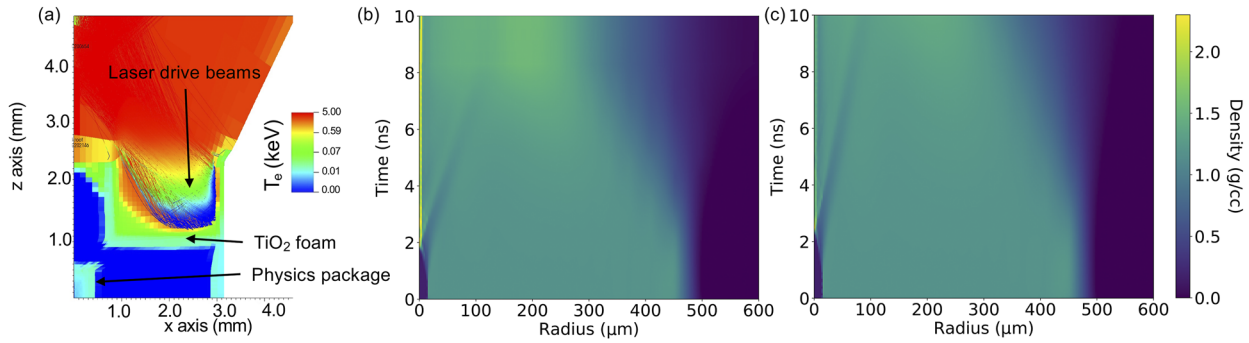


**FIG. 3.** Results of fully integrated hydrodynamic simulations using the Hydra code.[19] (a) Simulation of one quadrant of the hohlraum near the end of the 2 ns-long drive. The laser energy is almost completely absorbed inside the $TiO_2$ foam, heating it to temperatures of up to 5 keV. In this simulation, the physics package at the center of the thermo-mechanical package reaches a temperature of 8 eV. (b) Density evolution of the channel and surrounding plastic as a function of time and radius calculated for 8 eV heating of the plastic coating and (c) 4 eV (half drive) heating of the plastic coating. The simulations depict a shock wave launched outward into the plastic and a rarefaction wave propagating into the cylinder.

were chosen for their demonstrated high laser to x-ray conversion efficiency, up to 5%.[18] The absorption length of the x rays emitted from the foams is matched to the sample radius to ensure heating uniformity. The generated x rays will be absorbed by the physics package, heating it to ~8 eV [Fig. 3(a)].

## B. Backlighter and slit aperture setup

Sixteen NIF beams will be pointed onto a 10 $\mu$m thick Cu foil, which serves as the backlighter for this experiment (Fig. 2). Irradiation of the Cu foil with the laser beams will generate Cu He-$\alpha$ x rays (8.35 keV) that will pass through a 1 × 50 $\mu m^2$ slit aperture placed 10 mm downstream toward the main target. The slit is milled into a 50 $\mu$m thick Ta plate that tapers on the side facing the target to 10 × 50 $\mu m^2$ (for a detailed description, see Ref. 15). The slit is fabricated by a focused ion beam (FIB) at the University of Nevada, Reno. The slit will be filled with CH to absorb the soft x-ray load at the wide end of the slit and hence delay slit closure. The spatial-coherence requirement for diffraction-based imaging constrains the slit size, which must be on the order of a few micrometers or less.[20] Because of this, the slit will also diffract the transmitted x rays. We calculated the diffraction parameter of the slit to be $\sqrt{10\ \text{mm} \times 1.485\ \text{Å}} = 1.2\ \mu$m. This is comparable to the slit width of 1 $\mu$m; thus, we will be in the Fresnel regime with diffraction angles of the order of 1.48 Å/1 $\mu$m ≈ 0.1 mrad. However, the slit (even accounting for its 50 $\mu$m thickness) will transmit a broad range (~0.2 rad) of photon angles from a typical 1.2 mm diameter backlighter source size, which will result in complete blurring of the slit diffraction pattern. Thus, the slit will produce a partially coherent point-like source with a source spread function of ~1 $\mu$m.

## C. Diagnostics

A gated x-ray detector (GXD) with 240 ps integration time will record the radiography signal across four microchannel plate (MCP) strips that can be independently timed. The GXD is located 905 mm away from the target, yielding a large magnification of M = (905 + 14 mm)/14 mm = 65.6 and ensuring that diffraction features are visible given the ~50 $\mu$m point spread function of the MCP. A 50 $\mu$m thick W wire will be placed at the exit window (225 $\mu$m offset from the direct line of sight). This wire will help to determine the effective source function and spatial scale of the recorded image. Furthermore, the DANTE diagnostics at NIF will record the temporal evolution of the Ti K-shell emission, thermal emission, and hard-ray emission from the target drive.

## D. 2PP printed physics package

At the center of the TMP is the physics package, a 1000 $\mu$m diameter, 1.5 mm tall plastic cylinder with a 30 $\mu$m diameter channel running through the center [Fig. 4(a)]. Creating such a small feature is extremely challenging with conventional milling techniques; however, it can be accomplished with 2 Photon-Polymerization (2PP) techniques. The 2PP additive manufacturing process utilized a femtosecond laser and optical system to achieve ellipsoid-shaped polymerized voxels on a micrometer scale, which are overlapped along the length of the inner channel in 50 nm steps by translating the part with a precision direct drive linear motor stage.

As the goal of the experiment is to measure transport properties at the material interface between deuterium and plastic, it is vital that the interface is not rough to begin with. A surrogate sample to measure the roughness of the inner channel was fabricated by printing a semi-cylinder with the same printing parameters as the full cylinder. The semi-cylinder was imaged with scanning electron microscopy [Fig. 4(b)], and a surface roughness of sub 50 nm was measured in the exposed channel with a white light interferometer at multiple points [Fig. 4(c)]. The 2PP cylinder encapsulates a 30 $\mu$m diameter channel that is connected to a reservoir on top of the cylinder [Fig. 4(a)]. The reservoir is attached to a fill tube that is used to fill the channel with cryogenic cooled $D_2$ ($\rho$ = 0.19 g/cm$^3$). The plastic cylinder will be slowly cooled down, and the $D_2$ gas will condense within the channel and reservoir. The TMP itself will be low-level gas filled with He (<0.03 mg/cc) as a requirement for the temperature equilibration (the target is fielded at 21 K). The CH cylinder ($\rho$ = 1.15 g/cm$^3$) is made out of 60% bisphenol A ethoxylate diacrylate ($C_{20}H_{26}O_6$) and 40% dipenta erythritol penta-/hexa-acrylate ($C_{25}H_{32}O_{12}$).

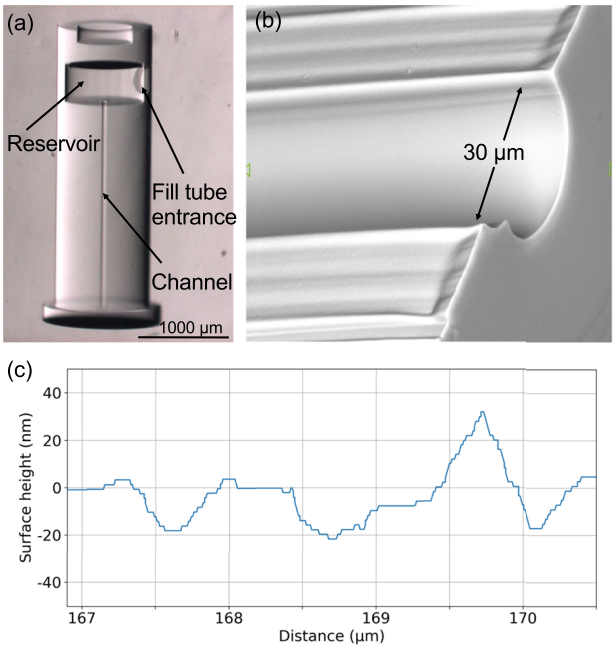


**FIG. 4.** (a) X-ray image of the 2PP printed cylinder along channel axis, including the 1.5 mm long and 30 $\mu$m in diameter channel holding the liquid $D_2$. The reservoir above the channel is 500 $\mu$m in diameter, 170 $\mu$m in height, and the fill tube entrance is 150 $\mu$m in diameter. The total diameter of the cylinder is 1000 $\mu$m. (b) Scanning electron microscopy image of the channel that was printed only one-sided. (c) Lineout of the measured surface roughness of the channel.

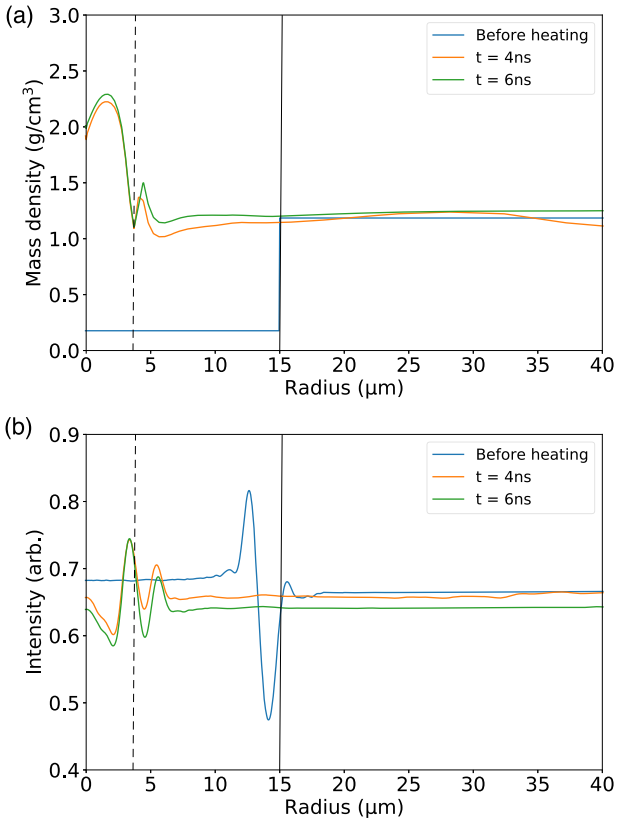


**FIG. 5.** (a) Density lineouts at three different probe times. The lineouts show the evolution of the density profile across the $D_2$ channel due to compression by the heated 2PP printed cylinder. The liquid $D_2$ column is compressed by ~10× to ~2.3 g/cm$^3$. After a few reverberations, a quasi-steady state is reached at ~4 ns due to pressure equilibration between the $D_2$ and the surrounding plastic. (b) Simulated diffraction patterns derived from the predicted density lineouts. The solid black line represents the interface between $D_2$ and plastic at ambient state, the dashed line the interface at driven state.

## III. SIMULATIONS

Radiation-hydrodynamic simulations showing the evolution of the target have been performed with Hydra.[19] First, the 2PP printed cylinder will be heated by the Ti He K-shell x rays, which ultimately lead to propagating shocks and rarefaction waves in the plastic cylinder and $D_2$ channel (Fig. 3). After the first 2 ns, the temperature of the plastic will rise to approximately ~8 eV, leading to the compression of the central channel and an increase of the $D_2$ density to ~2.3 g/cm$^3$ [Fig. 3(b)]. At this point, the interface between $D_2$ and plastic will stagnate, after which the evolution of the density profile is driven by transport properties, namely thermal conduction and particle diffusion. As heat flows from the plastic into the $D_2$, we observe an increase in the density of the plastic next to the interface and a corresponding decrease in the $D_2$ density.[13,21] At the same time, particle diffusion acts to smooth out the density jump at the interface itself. Lineouts showing the evolution of the density profile across the channel are depicted in Fig. 5(a). The expected diffraction patterns are shown in Fig. 5(b), which combine the complex transmission function of the target with the optical transfer function for Fresnel diffraction. A sharp fringe contrast at the $D_2$/plastic interface is expected, which will ultimately move to smaller radii at later probe times. At 4 ns, the conductivity-sensitive diffraction peaks are located at ~3 $\mu$m radius. Parameterization of the diffraction signal will be used to obtain information on the density profile and will help to determine the scale-length of thermal conduction in the $D_2$ and plastic. All calculations assumed a 1 $\mu$m source size and were performed with the predicted density evolution shown in Fig. 5(a). Further details of the diffraction calculation can be found in Pogany *et al.*[22]

In addition, we have simulated a low laser drive [Fig. 3(c)], which assumes that only half of the drive energy is delivered into the $TiO_2$ foams. In this case, the plastic is only heated to ~4 eV, leading to a density increase of the $D_2$ to ~1.7 g/cm$^3$. As the outgoing shock wave scales quite strongly with the drive (17.5 km/s for the high drive and 10.5 km/s for the low drive), we will be able to use this information to infer sample temperature. Furthermore, our simulations show that the target survives at least 10 ns in both laser drive cases before the incoming rarefaction wave reaches the $D_2$ channel.

## ACKNOWLEDGMENTS

Lawrence Livermore National Laboratory is operated by Lawrence Livermore National Security, LLC, for the U.S. Department of Energy, National Nuclear Security Administration under

Contract No. DE-AC52-07NA27344 and supported by Laboratory Directed Research and Development (LDRD) (Grant No. 21-ERD-029). This document was prepared as an account of work sponsored by an agency of the U.S. Government. Neither the U.S. Government nor Lawrence Livermore National Security, LLC, nor any of their employees makes any warranty, expressed or implied, or assumes any legal liability or responsibility for the accuracy, completeness, or usefulness of any information, apparatus, product, or process disclosed, or represents that its use would not infringe privately owned rights. Reference herein to any specific commercial product, process, or service by trade name, trademark, manufacturer, or otherwise does not necessarily constitute or imply its endorsement, recommendation, or favoring by the U.S. Government or Lawrence Livermore National Security, LLC. The views and opinions of authors expressed herein do not necessarily state or reflect those of the U.S. Government or Lawrence Livermore National Security, LLC, and shall not be used for advertising or product endorsement purposes. This material is based upon work supported by the National Science Foundation under Grant No. PHY-2045718.

## AUTHOR DECLARATIONS

### Conflict of Interest

The authors have no conflicts to disclose.

### Author Contributions

**M. O. Schoelmerich**: Conceptualization (lead); Data curation (lead); Writing – original draft (lead); Writing – review & editing (lead). **T. Döppner**: Conceptualization (lead); Data curation (equal); Funding acquisition (lead); Investigation (equal); Methodology (equal); Writing – review & editing (equal). **C. H. Allen**: Investigation (lead); Methodology (equal); Visualization (equal); Writing – review & editing (equal). **L. Divol**: Data curation (equal); Formal analysis (equal); Investigation (equal); Software (equal); Visualization (equal); Writing – review & editing (equal). **M. Oliver**: Conceptualization (equal); Formal analysis (equal); Investigation (equal); Writing – review & editing (equal). **D. Haden**: Conceptualization (equal); Data curation (equal); Investigation (equal); Writing – review & editing (equal). **M. Biener**: Conceptualization (equal); Investigation (equal); Methodology (equal). **J. Crippen**: Methodology (equal). **J. Delora-Ellefson**: Methodology (equal). **B. Ferguson**: Methodology (equal). **D. Gericke**: Conceptualization (equal); Investigation (equal); Methodology (equal). **A. Goldman**: Methodology (equal). **A. Haid**: Methodology (equal). **C. Heinbockel**: Methodology (equal). **D. Kalantar**: Conceptualization (equal); Methodology (equal); Writing – review & editing (equal). **Z. Karmiol**: Methodology (equal). **G. Kemp**: Methodology (equal). **J. Kroll**: Methodology (equal). **O. L. Landen**: Methodology (equal). **N. Masters**: Methodology (equal). **Y. Ping**: Conceptualization (equal); Investigation (equal); Methodology (equal); Writing – review & editing (equal). **C. Spindloe**: Methodology (equal). **W. Theobald**: Conceptualization (equal); Investigation (equal); Methodology (equal). **T. G. White**: Conceptualization (lead); Data curation (equal); Formal analysis (equal); Funding acquisition (lead); Investigation (equal); Methodology (equal); Project administration (equal); Writing – original draft (equal); Writing – review & editing (equal).

## DATA AVAILABILITY

The data that support the findings of this study are available within the article.

## REFERENCES

[1] T. Guillot, Science **286**, 72 (1999).
[2] C. Paquette, C. Pelletier, G. Fontaine, and G. Michaud, Astrophys. J., Suppl. Ser. **61**, 177 (1986).
[3] S. Atzeni and J. Meyer-ter Vehn, *The Physics of Inertial Fusion: Beam Plasma Interaction, Hydrodynamics, Hot Dense Matter* (OUP Oxford, 2004), Vol. 125.
[4] J. Kress, J. S. Cohen, D. Horner, F. Lambert, and L. Collins, Phys. Rev. E **82**, 036404 (2010).
[5] J. L. Milovich, P. Amendt, M. Marinak, and H. Robey, Phys. Plasmas **11**, 1552 (2004).
[6] C. Wang, Z. Li, D. Li, and P. Zhang, Phys. Plasmas **22**, 102702 (2015).
[7] A. McKelvey, G. Kemp, P. Sterne, A. Fernandez-Panella, R. Shepherd, M. Marinak, A. Link, G. Collins, H. Sio, J. King *et al.*, Sci. Rep. **7**, 7015 (2017).
[8] Y. Ping, H. D. Whitley, A. McKelvey, G. E. Kemp, P. A. Sterne, R. Shepherd, M. Marinak, R. Hua, F. N. Beg, and J. H. Eggert, Phys. Rev. E **100**, 043204 (2019).
[9] T. G. White, "Study of high energy density matter through quantum molecular dynamics and time resolved x-ray scattering," Ph.D. thesis, Oxford University, UK, 2014.
[10] L. Wollenweber, T. R. Preston, A. Descamps, V. Cerantola, A. Comley, J. H. Eggert, L. B. Fletcher, G. Geloni, D. O. Gericke, S. H. Glenzer *et al.*, Rev. Sci. Instrum. **92**, 013101 (2021).
[11] E. E. McBride, T. G. White, A. Descamps, L. B. Fletcher, K. Appel, F. P. Condamine, C. B. Curry, F. Dallari, S. Funk, E. Galtier *et al.*, Rev. Sci. Instrum. **89**, 10F104 (2018).
[12] E. I. Moses, Fusion Eng. Des. **85**, 983 (2010).
[13] Y. Ping, O. L. Landen, D. G. Hicks, J. A. Koch, R. Wallace, C. Sorce, B. A. Hammel, and G. W. Collins, J. Instrum. **6**, P09004 (2011).
[14] E. L. Dewald, O. L. Landen, L. Masse, D. Ho, Y. Ping, D. Thorn, N. Izumi, L. Berzak Hopkins, J. Kroll, A. Nikroo, and J. A. Koch, Rev. Sci. Instrum. **89**, 10G108 (2018).
[15] C. H. Allen, M. Oliver, L. Divol, O. L. Landen, Y. Ping, M. Schölmerich, R. Wallace, R. Earley, W. Theobald, T. G. White, and T. Döppner, Appl. Opt. **61**, 1987 (2022).
[16] M. Oliver, C. H. Allen, L. Divol, Z. Karmiol, O. L. Landen, Y. Ping, R. Wallace, M. Schölmerich, W. Theobald, T. Döppner, and T. G. White, Rev. Sci. Instrum. **93**, 093502 (2022).
[17] A. Zylstra, O. Hurricane, D. Callahan, A. Kritcher, J. Ralph, H. Robey, J. Ross, C. Young, K. Baker, D. Casey *et al.*, Nature **601**, 542 (2022).
[18] M. May, G. Kemp, R. Benjamin, P. Poole, K. Widmann, J. Colvin, T. Fears, F. Qian, and B. Blue, in *2021 IEEE International Conference on Plasma Science (ICOPS)* (IEEE, 2021), p. 1.
[19] M. M. Marinak, R. E. Tipton, O. L. Landen, T. J. Murphy, P. Amendt, S. W. Haan, S. P. Hatchett, C. J. Keane, R. McEachern, and R. Wallace, Phys. Plasmas **3**, 2070 (1996).
[20] G. Margaritondo and G. Tromba, J. Appl. Phys. **85**, 3406 (1999).
[21] B. A. Hammel, S. W. Haan, D. S. Clark, M. J. Edwards, S. H. Langer, M. M. Marinak, M. V. Patel, J. D. Salmonson, and H. A. Scott, High Energy Density Phys. **6**, 171 (2010).
[22] A. Pogany, D. Gao, and S. W. Wilkins, Rev. Sci. Instrum. **68**, 2774 (1997).